Rapid Probe Engagement and Withdrawal With Force Minimization in Atomic Force Microscopy: A Learning-Based Online-Searching Approach

Jingren Wang and Qingze Zou

***Abstract*—In this article, the problem of rapid probe engagement and withdrawal in atomic force microscopy (AFM) is addressed. Probe engagement and withdrawal is needed in almost all AFM operations, ranging from imaging to nanomanipulation. However, due to the highly nonlinear force–distance relation, large probe–sample interaction force can be induced during the probe engagement and withdrawal process, resulting in sample deformation and damage and measurement errors. Rapid probe engagement and withdrawal is needed to achieve high-speed AFM operations, particularly, to capture and interrogate dynamic evolutions of the sample. We propose an online-searching-based optimization approach to minimize both the engagement (and withdrawal) time and the interaction force. The force–displacement profile of the probe is partitioned and then optimized sequentially, by immersing optimal trajectory design and iterative learning control into the Fibonacci search process. The proposed approach is illustrated through experimental implementations on two different types of polymer species, a polydimethylsiloxane sample, and a dental silicone sample, respectively.**

***Index Terms*—Fibonacci search, high-speed atomic force microscopy, iterative learning control, real-time optimization.**

I. Introduction

In THIS article, rapid probe engagement and withdrawal with probe–sample interaction force minimized in atomic force microscope (AFM) operation is studied. Probe engagement and withdrawal is needed in almost all AFM operations, ranging from imaging [1], nanomechanical properties measurement/mapping [2], to nanomanipulation [3]. During the engagement and withdrawal process, the "snap-in" [4] force followed by a large repulsive overshoot [5], and a large adhesive force [6] can be induced, respectively. When the sample is soft, the sample can be stretched and/or compressed by these forces, resulting in not only sample deformation and damage, but also artifacts in the AFM measurement results.

Probe engagement and withdrawal without inducing large probe–sample interaction force is needed in AFM operations, particularly for soft live biological specimens. Due to the highly nonlinear force–distance relation involved [7], large probe–sample interaction force can be induced when the probe is engaged to and/or withdrawn from the sample surface at high speed [4]. Rapid probe engagement and withdrawal, however, is especially critical in AFM applications with frequent probe engagements and withdrawals, e.g., in piecewise-scanning-based imaging [1], [8] and discrete nanomechanical mapping [2]. The importance is more pronounced when measuring dynamic evolutions of soft live biological specimens, for example, when mapping the time-varying mechanical properties of a live cell membrane during the endocytosis process [9], or those of guard cells during the opening and closing processes of a stoma on a plant leaf [10]. Rapid probe engagement and withdrawal is needed to quickly reach the desired initial measurement condition at each sampling location, and leave that location without inducing sample deformation or damage before and after the measurement. Therefore, there are needs to achieve rapid probe engagement and withdrawal while minimizing the interaction force.

Achieving such an operation, however, is challenging. During the engagement, the probe is initially driven by the highly nonlinear attractive Van der Waals force [11], followed by the repulsive dominant force. As a result, it is difficult to steer the probe away from the "snap-in" and the overshoot force region, to reach a stable contact at the desired force load [4]. During the withdrawal, the probe undergoes a reverse switch from the repulsive to the attractive dominant force, followed by a sudden probe–sample separation [4]. Such an unstable probe "pull-off" induces a large adhesive force [12] followed by post-withdrawal oscillations. Moreover, the probe–sample interaction force tends to increase significantly as the engagement/withdrawal rate increases [4], [12]. Although such rapid and large changes of the probe–sample interaction might be alleviated by using vertically mounted cantilever [13], this approach is incompatible with the existing standard AFM systems, and moreover, largely limits the speed of AFM and its use in general applications. Therefore, to achieve rapid

Manuscript received July 7, 2019; revised November 6, 2019 and January 27, 2020; accepted January 28, 2020. Date of publication February 4, 2020; date of current version April 15, 2020. Recommended by Technical Editor I.-M. Chen. This work was supported by the NSF under Grants IDBR-1353890, CMMI 1663055, and 1851907. *(Corresponding author: Qingze Zou.)*

The authors are with the Department of Mechanical and Aerospace Engineering, Rutgers, The State University of New Jersey, Piscataway, NJ 08854 USA (e-mail: jw986@scarletmail.rutgers.edu; qzzou@soe.rutgers.edu).

Color versions of one or more of the figures in this article are available online at https://ieeexplore.ieee.org.

Digital Object Identifier 10.1109/TMECH.2020.2971464

probe engagement and withdrawal, the highly nonlinear probe–sample interaction and rapid attractive–repulsive transition must be addressed.

The main contribution of this article is the development of a learning-based, online-searching optimization approach to achieve rapid probe engagement and withdrawal on soft samples. The basic idea is to partition the engagement and the withdrawal process into different phases—based on the inherent characteristics of the probe–sample interaction, and then decouple and separate the time and force minimization through a sequential optimization process. For example, in one phase, the main objective it is to minimize the interaction force, while in the other phase, it is to minimize the time while maintaining the already-minimized force largely unchanged. Thus, the complexity and robustness issues due to the highly nonlinear probe sample interaction are simplified. Specifically, a Fibonacci-based iterative searching (FIS) process is proposed to online minimize the fore or the time, where the optimal transition trajectory design [14] and the modeling-free inversion-based iterative control technique [15] are immersed in the online search process [16], [17]. This approach is illustrated by implementing it through AFM experiment on a polydimethylsiloxane (PDMS) sample and a dental silicone sample, respectively. As one of the first few works on rapid engagement and withdrawal with force minimization, this article is built upon and extends our recent preliminary results in [18], by further simplifying and optimizing the proposed approach, and providing more enriched and broader experimental examples.

II. Rapid Engagement and Withdrawal With Online Probe–Sample Interaction Force Minimization

A. Probe Engagement and Withdrawal on Soft Samples: Issues and Challenges

During the engagement and withdrawal process, as the probe (driven by the z-axis piezo actuator) approaches to or withdraws from the sample, the pair-potential energy $E(z)$ and the probe–sample interaction force $F(z)$, can be characterized, respectively, by the Lennard–Jones model [7] as

$$E(z) = 4\varepsilon\left[\left(\frac{\sigma}{z}\right)^{12} - \left(\frac{\sigma}{z}\right)^{6}\right], \qquad F(z) = \frac{dE(z)}{dz} \quad (1)$$

where z is the probe–sample distance, and ε and σ are the material-dependent constants, respectively. The first and second terms, $(\sigma/z)^{12}$ and $(\sigma/z)^{6}$ of $E(z)$, describe the change of the energy in the repulsive and the attractive interaction regions, respectively.

The above Lennard-Jones model in (1) clearly captures the stiff nonlinearity of the probe–sample interaction during the probe engagement/withdrawal process, and speaks directly to the control challenges involved. Due to a highly nonlinear force–distance relation—the force is inverse proportional to the distance of over six order [see (1)], linearization-based approach becomes ineffective. Moreover, model-based nonlinear control also faces difficulty in modeling and robustness. It is difficult to obtain an accurate model of the probe–sample interaction in engagement and withdrawal, as such a model depends on not only the characteristics of the probe and the mechanical properties of the sample, but also the measurement environment and the engagement and withdrawal process itself. Furthermore, such a high-order stiff nonlinear dynamics also implies that the dynamics model is highly sensitive to the parameters of the probe and/or the sample, and thereby lacks robustness in practical implementations, i.e., it is practically infeasible to update/correct the model when the AFM probe is modified (due to wear) or replaced. Therefore, to overcome the limitations of the model-based nonlinear control approach, we propose a learning-based online-searching optimization approach.

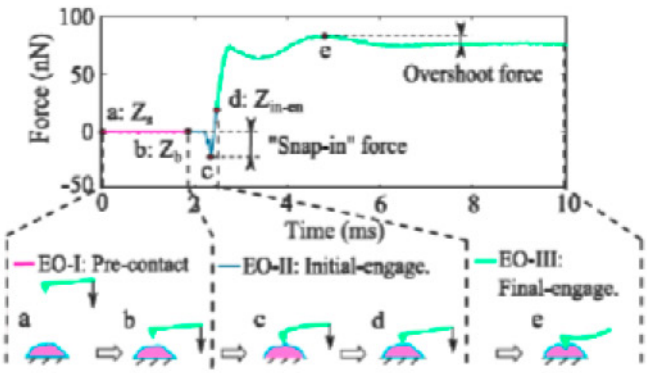

Fig. 1. (Top) Force–time profile of probe engagement, where the "snap-in" and overshoot force are marked out, respectively, and (bottom) the partition of the three phases (marked out by the vertical dashed lines), where "a"–"e" mark out the characteristic positions of the probe (as schematically depicted in bottom plots), of which "a" (Z_s), "b" (Z_b), and "d" (Z_{in-en}) are used later, respectively.

B. Rapid Probe Engagement and Withdrawal: Objectives

We start by describing the partition of the engagement and the withdrawal processes each into three different phases, respectively. Specifically, the engagement process is partitioned as follows.

1) *EO-I: Precontact phase*, during which the probe is transited from the initial position, Z_s (relatively far away from the sample), to the position right above the onset of the tip–sample interaction occurs (called the *tip–sample interaction border*, Z_b, below; see Fig. 1).
2) *EO-II: Initial-engagement phase*, during which the probe is transited from the tip–sample interaction border to the stable contact position with a prechosen preload (called the *initial engagement position*, $Z_{\text{In-en}}$, below; see Fig. 1).
3) *EO-III: Final-engagement phase*, during which the probe is transited from the initial engagement position to contact the sample with desired force load amplitude (see Fig. 1).

The withdrawal process is also partitioned into three phases.

1) *WO-II: Repulsive withdrawal phase*, during which the probe is pulled up from the original contact position to the position where the interaction force is close to zero, that signals the transition from the repulsive to the attractive region (called the *end-of-repulsive position*, $Z_{\text{ee,r}}$, below; see Fig. 2).

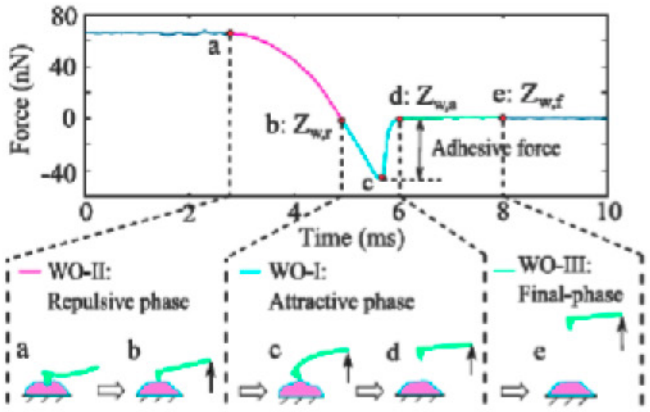

Fig. 2. (Top) Force–time profile of probe withdrawal, where the adhesive force is marked out, and (bottom) the partition of the three phases, where "a"–"e" mark out the characteristic positions of the probe (as schematically depicted in bottom plots), of which "b" ($Z_{w,r}$), "d" ($Z_{w,a}$), and "e" ($Z_{w,f}$) are used later, respectively.

2) *WO-I: Attractive withdrawal phase*, during which the probe is withdrawn from the end-of-repulsive position to the position where the interaction force becomes negligible (called the *loss-of-contact position*, $Z_{w,a}$, below; see Fig. 2);
3) *WO-III: Final withdrawal phase*, during which the probe is transited from the loss-of-contact position to the final position well above the sample surface, $Z_{w,f}$ (for conducting the required operation next, see Fig. 2).

Moreover, in the rest of the article, we called the displacement of the cantilever the *probe displacement* (measured by the z-axis displacement sensor), and the interaction force the *probe force* (measured via the cantilever deflection). Thus, with these partitions, the following objectives are proposed.

Optimal Rapid Probe Engagement:

1) *Objective EO-I*: During the precontact phase, achieve a rapid optimal transition (specified below immediately) of the probe displacement from the initial position to the tip–sample interaction border, and then further minimize the total precontact time.
2) *Objective EO-II*: In the initial-engagement phase, achieve a rapid optimal transition of the probe displacement, and optimize the initial-engagement time (i.e., the time period corresponding to this phase), such that the *peak "snap-in" force*, i.e., the maximum attractive force, is minimized.
3) *Objective EO-III*: In the final-engagement phase, achieve a rapid optimal transition of the probe force, and optimize the final engagement time (i.e., the time period corresponding to this phase) to minimize the cost function

$$J_{d_{en}}(\|F_{os}(\cdot)\|_\infty, T_{en}) = \gamma_1 \|F_{os}(\cdot)\|_\infty + \gamma_2 T_{en} \tag{2}$$

where $\|\cdot\|_\infty$ denotes the $\ell-\infty$ norm, $F_{os}(t)$ is the repulsive force (called the *overshoot force* below, $\|F_{os}(\cdot)\|_\infty$ is called below the *peak overshoot force*), with T_{en} the final-engagement time, and $\gamma_1 > 0$, $\gamma_2 > 0$ are the weights, respectively.

Definition 1: Optimal Transition of Probe Displacement For a given transition period T_{tr}, an optimal transition of the probe displacement is achieved if

1) The vibration of the probe displacement is minimized in the sense of energy minimization

$$\min J_z(T_{tr}) = \min \int_0^{T_{tr}} \xi(t)^T Q \xi(t) d\tau \tag{3}$$

where $\xi(t) = [z(t), \dot{z}(t)]^T$ with $z(t)$ and $\dot{z}(t)$ the probe displacement and velocity, respectively, and $Q \in \Re^{2\times 2}$ is a positive definite matrix.
2) No posttransition oscillation of the probe displacement is induced.

Optimal Probe Force Transition is defined similarly by replacing "displacement" with "force" in the above definition.

Optimal Probe Withdrawal: As the adhesive force is highly coupled with the total withdrawal time, a tradeoff between the adhesive force and the total withdrawal time becomes necessary. Thus, we propose to minimize the peak adhesive force first, and then the total withdrawal time afterward, without increasing the peak adhesive force.

1) *Objective WO-I*: In the attractive withdrawal phase, optimize the probe velocity of a constant-velocity probe displacement trajectory in this phase, to minimize the peak adhesive force without increasing the withdrawal time in the other two phases.
2) *Objective WO-II*: In the repulsive withdrawal phase, optimize the end-of-repulsive position, $Z_{w,r}$, such that the following cost function is minimized, under the constraint that the peak adhesive force, $\|F_{Adh}(\cdot)\|_\infty$ is maintained, closely around its optimal level achieved in Objective WO-I above, $\mathbf{F}^*_{Adh}$

$$J_{z_w}(\|F_{Adh}(\cdot)\|_\infty, T_w) = \beta_1 \|F_{Adh}(\cdot)\|_\infty + \beta_2 T_w \quad \text{with} \quad \left|\|F_{Adh}(\cdot)\|_\infty - \mathbf{F}^*_{Adh}\right| \le \epsilon_{adh} \tag{4}$$

where $F_{Adh}(\cdot)$ is the adhesive force measured during the entire withdrawal process, T_w is the total withdrawal time, $\beta_1 > 0$, $\beta_2 > 0$ are the weights, and ϵ_{adh} is a prechosen threshold, respectively.
3) *Objective WO-III*: In the final withdrawal phase, achieve a rapid optimal transition of the probe displacement, and optimize the loss-of-contact position, $Z_{w,a}$, to minimize the constrained cost function in (4) such that the total withdrawal time is further minimized.

The same cost function (4) is employed in both Objectives WO-II and WO-III with different weights, as reduction of the withdrawal time can reversely increase the peak adhesive force.

Next, we propose to seek the optimal parameters in Objectives EO-II, EO-III, WO-I, WO-II, and WO-III, respectively, through a learning-based online-searching approach. We present by showing how each of the objectives is achieved in order.

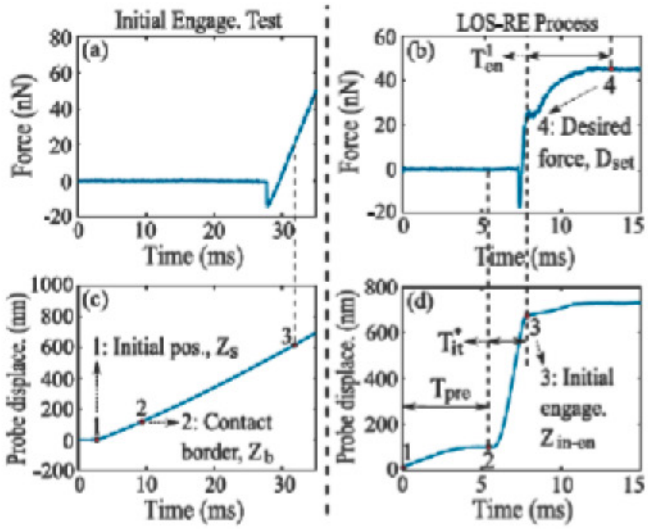

Fig. 3. Example of (a) the force and (c) probe displacement profile measured in an initial engagement test to quantify the characteristic probe positions (marked by 1, 2, 3), and (b) the force and (d) displacement profile (with the desired force load marked by 4) designed by using the proposed LOS-RE process using those positions quantified in (a) and (c), respectively.

C. Optimal Rapid Probe Engagement: A Learning-Based, Online-Searching Optimization

We propose a learning-based online-searching (LOS) technique for rapid probe engagement and withdrawal (called *LOS-RE* and *LOS-RW* below, respectively) [18]. First, the characteristic probe positions are estimated through an initial test to identify the three phases of the engagement.

1) Estimation of the Probe–Sample-Contact Boundary Positions: By measuring the force–displacement profile during an engagement process at low speed, the following probe positions are estimated [see Fig. 3(a) and (c)]: a) The initial probe position, Z_s; b) the tip–sample interaction border, Z_b; and c) the initial engagement position, $Z_{\text{in-en}}$. The quantification of probe positions above is robust, as its uncertainty can be accounted for by the "buffer" zone (i.e., the small vicinity above the tip–sample interaction). Thus, accurate identification of the probe position where the "snap-in" occurs is not needed.

2) Objective EO-I: Rapid Precontact Probe Approach: The goal in Objective EO-I is to dramatically reduce the probe travel time before the probe–sample contact. This probe travel time is rather large in conventional engagement, where to avoid the probe/sample deformation and damage, the speed is conservative. We propose to, first, design the desired transition trajectory of the probe displacement, and then track the desired trajectory accurately.

Objective EO-I.1: Optimal transition trajectory design in the precontact phase. The desired probe displacement trajectory for the precontact phase is designed online using the optimal transition trajectory design technique [14], [19]. Specifically, given the precontact time T_{pre}, and the starting and final probe position of the precontact, $z(0) = Z_s$ and $z(T_{\text{pre}}) = Z_b$, respectively [see Fig. 3(d)], the optimal transition trajectory [from $z(0)$ to $z(T_{\text{pre}})$] is obtained from the solution that minimizes the cost function in (3) [14], [19], as the (first) state trajectory of the following system:

$$\dot{\xi}(t) = (I_{\text{up}} + B_\xi H_\xi)\xi(t) + B_\xi \gamma(t) \triangleq \hat{A}_\xi \xi(t) + B_\xi \gamma(t) \quad (5)$$

under the optimal "input" $\gamma^*(t)$

$$\gamma^*(t) = R^{-1} B_\xi^T e^{\hat{A}_\xi^T (T_{\text{pre}} - t)} \mathscr{G}^{-1}(T_{\text{pre}}) \times \left[\xi(T_{\text{pre}}) - e^{\hat{A}_\xi (T_{\text{pre}} - 0)} \xi(0)\right] \quad (6)$$

where, respectively, $I_{\text{up}} = \left[\begin{smallmatrix} 0 & 1 \\ 0 & 0 \end{smallmatrix}\right]$, $B_\xi = [0\ 1]^T$, $H_\xi \in \Re^{1\times 2}$ is chosen such that $\hat{A}_\xi$ is Hurwitz, $\mathscr{G}(T_{\text{pre}})$ is the controllable Gramian for $\{\hat{A}_\xi, B_\xi\}$

$$\mathscr{G}(T_{\text{pre}}) = \int_0^{T_{\text{pre}}} e^{\hat{A}_\xi (T_{\text{pre}} - \tau)} B_\xi R^{-1} B_\xi^T e^{\hat{A}_\xi^T (T_{\text{pre}} - \tau)} d\tau. \quad (7)$$

In the following sections, we denote the optimal transition trajectory obtained with a given boundary condition $B_{of} \triangleq (\xi(0), \xi(T_{\text{tr}}))$ and given transition time T_{tr} as $\Phi(t, B_{\text{of}}, T_{\text{tr}})$, i.e.

$$(B_{of}, T_{tr}) \xrightarrow[\text{Trajectory design}]{\text{Optimal transition}} \Phi(t, B_{of}, T_{\text{tr}}). \quad (8)$$

For example, the above optimal transition trajectory for the precontact phase is given as $\Phi(t, B_{\text{of}}, T_{\text{pre}})$.

Objective EO-I.2: Tracking of the designed transition trajectory via online iterative learning. The optimal transition trajectory of the probe displacement, $\Phi(t, B_{\text{of}}, T_{\text{pre}})$, is tracked via iterative learning control technique. The control input (i.e., the voltage profile applied to the z-axis piezo actuator), $u_z^*(t)$, is obtained through the modeling-free iterative learning control (MIIC) technique online during the engagement process. The MIIC algorithm [15] is described in Appendix A.

Rapid precontact is achieved by choosing a fast enough precontact time T_{pre} in the above two steps (Objectives EO-I.1 and EO-I.2). To further minimize the precontact time period, T_{pre}, the total transition time $T_{\text{tr}} = T_{\text{pre}}$, reduced in a bisection search manner is used to redesign the desired optimal transition trajectory $\Phi(t, B_{\text{of}}, T_{\text{pre}})$ in Objective EO-I.1, and then tracked via the MIIC above, until the tracking error exceeds the threshold value.

3) Objective EO-II: Online Optimization of the Initial-engagement Displacement Profile with Minimal "Snap-in" Force: Under the condition that the tip–sample interaction border has been achieved (Objective EO-I), the peak "snap-in" force is online-minimized through a FIS process—without accurately modeling the probe–sample interaction. As depicted in Fig. 4, the FIS process is described as an algorithm below.

FIS Process. In each jth search/update of the FIS process:

1) Design the desired initial-engagement probe displacement profile, $z_{tr2en}^j(\cdot)$, by using the chosen method; for example, the optimal transition trajectory design [see (8)]

$$z_{tr2en}^j(t) = \Phi(t, B_{\text{of}}^j, T_{\text{it}}^j), \quad \text{for } t \in [t_{\text{pre}}, t_{\text{in-en}}^j] \quad (9)$$

with the given boundary condition $B_{\text{of}}^j = (\xi(t_{\text{pre}}), \xi(t_{\text{in-en}}^j))$, and the jth initial-engagement time, $T_{\text{it}}^j =$

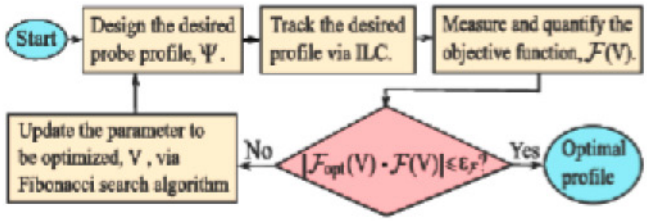

Fig. 4. Flow chart of the proposed FIS process.

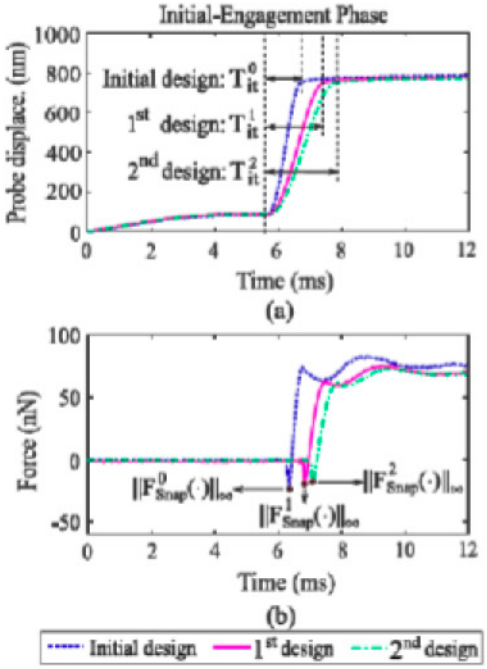

Fig. 5. Example of online optimization of the initial-engagement displacement profile through the FIS process, by (a) tuning the initial-engagement time period [marked out in (a)] of the probe displacement, $\Phi(t, B_{of}^j, T_{it}^j)$, to (b) minimize the "snap-in" force [marked out in (b)], $\|F_{Snap}^j(\cdot)\|_\infty$, via the Fibonacci search [see (10)].

$t_{in-en}^j - t_{pre}$, where t_{pre} and t_{in-en}^j are the starting and the final time instant of the jth initial-engagement, $\xi(t_{pre}) = [z(t_{pre}), \dot{z}(t_{pre})]^T$, $\xi(t_{in-en}^j) = [z(t_{in-en}^j), \dot{z}(t_{in-en}^j)]^T$, respectively.

2) Track the desired initial-engagement displacement profile, $z_{tr2en}^j(\cdot)$, by using the MIIC technique online, and measure the peak "snap-in" force, $\|F_{Snap}^j(\cdot)\|_\infty$ (see Fig. 5)

$$\text{Tracking}(\Phi(t, B_{of}^j, T_{it}^j)) \xrightarrow{\text{MIIC}} \|F_{Snap}^j(\cdot)\|_\infty. \quad (10)$$

3) Online update/optimize the corresponding initial-engagement time, T_{it}^j, through the online Fibonacci-based optimization process (see Appendix B), to minimize the peak "snap-in" force, $\|F_{Snap}^j(\cdot)\|_\infty$

$$T_{it}^{j+1} = \Gamma_{Fib}(\Phi(t, B_{of}^j, T_{it}^j), \|F_{Snap}^j(\cdot)\|_\infty) \quad \text{for } T_{it}^j \in [T_{it,l}^j, T_{it,h}^j]. \quad (11)$$

where, respectively, $T_{it,l}^j$ and $T_{it,h}^j$ are the lower and upper bounds of the searching interval of T_{it}^j. Then, the updated initial-engagement time, T_{it}^{j+1}, will be used in the design of the desired initial-engagement displacement profile, $z_{tr2en}^{j+1}(\cdot)$, to initiate the next FIS process.

4) Repeat the above three steps until convergence is reached: The difference between the Nth intermediate "optimal" peak "snap-in" force, $\|F_{Snap,opt}^N(\cdot)\|_\infty$, and the measured "snap-in" force, $\|F_{Snap}^N(\cdot)\|_\infty$, is within the prechosen threshold value, $\varepsilon_{Snap} > 0$, i.e., $\left|\|F_{Snap,opt}^N(\cdot)\|_\infty - \|F_{Snap}^N(\cdot)\|_\infty\right| \leq \varepsilon_{Snap}$.

4) Objective EO-III. Online Final-Engagement Force Profile Optimization: After both Objectives EO-I and EO-II have been achieved, the above FIS process is also utilized to online-minimize the overshoot force while keeping the engagement time small. Specifically, in the jth FIS searching/update process, the jth final-engagement time, T_{en}^j, is obtained by minimizing the cost function $J_{d_{en}}^j(\cdot)$ given in (2) as

$$T_{en}^j = \Gamma_{Fib}(\Phi(t, B_{of}^{j-1}, T_{en}^{j-1}), J_{d_{en}}^{j-1}(\|F_{os}^{j-1}(\cdot)\|_\infty, T_{en}^{j-1})) \quad (12)$$

where, respectively, $\Phi(\cdot)$ is the $(j-1)$th desired final-engagement force profile designed as in (8) above, with the given final-engagement time period, $T_{en}^{j-1} \in [T_{en,l}^{j-1}, T_{en,h}^{j-1}]$, and the boundary condition, $B_{of}^{j-1} = (\xi(t_{in-en}^*), \xi(t_{en}^{j-1}))$. $T_{en,l}^{j-1}$, $T_{en,h}^{j-1}$, are the lower and upper bound of the searching interval of $T_{en}^{j-1} = t_{en}^{j-1} - t_{in-en}^*$, and $\xi(t_{in-en}^*) = [d(t_{in-en}^*), \dot{d}(t_{in-en}^*)]^T$, $\xi(t_{en}^{j-1}) = [D_{set}, 0]^T$, where t_{en}^{j-1} is the final time instant in the preceding $(j-1)$th final-engagement process, and D_{set} is the desired force load, respectively. $\|F_{os}^{j-1}(\cdot)\|_\infty$ is the peak overshoot force, measured when $\Phi(\cdot)$ is tracked accurately by using the MIIC technique. The weights in the cost function $J_{d_{en}}^{j-1}(\cdot)$ are chosen to normalize the peak overshoot force and the final-engagement time, respectively.

During the FIS process, at the end of each iteration (of each design update), the probe is withdrawn from the sample, and repositioned at the tip–sample interaction border, Z_b, by using a PI feedback control. Then, the PI feedback control is switched off, and the next iteration starts immediately.

Finally, the optimal control inputs, each corresponding to Objectives EO-I, EO-II, and EO-III, respectively, are concatenated to yield the input for the entire engagement process. The smoothness of the desired probe profile across each phase is guaranteed by the boundary conditions used in the optimal transition trajectory design.

D. Optimal Rapid Probe Withdrawal via Learning-Based Online-Searching

The above learning-based online-searching approach is also extended to optimize the probe withdrawal process.

1) Obtain the Characteristic Probe Positions in the Withdrawal Process: As in the engagement process, the characteristic probe positions of the three withdrawal phases (see Section II-B) are quantified via experiment. Specifically, the desired probe displacement profile is designed via the optimal

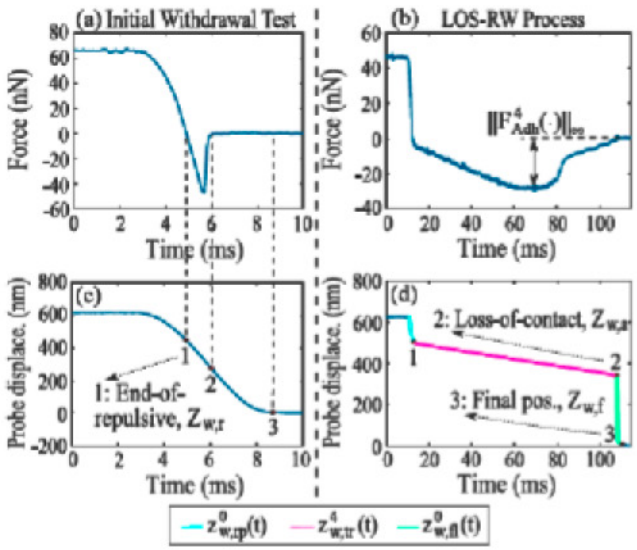

Fig. 6. Example of (a) the force and (c) probe displacement profile measured in an initial withdrawal test to quantify the characteristic probe positions (marked by 1, 2, 3), and (b) the force and (d) displacement profile designed by using the proposed LOS-RW process using those positions quantified in (a), (c), respectively.

transition trajectory design technique, $z_{w,\text{test}}(\cdot)$, and tracked by using the MIIC technique online

$$z_{w,\text{tost}}(t) = \Phi(t,\, B_{of},\, T_{w,\text{init}}), \qquad \text{for } t \in [0,\, T_{w,\text{init}}] \quad (13)$$

where $T_{w,\text{init}}$ is the given withdrawal time period, and $B_{of} = (\xi(0),\, \xi(T_{w,\text{init}}))$ is the boundary condition, with $\xi(0) = [z(0),\, 0]^T$, $\xi(T_{w,\text{init}}) = [Z_{w,f},\, 0]^T$, and $Z_{w,f}$ the final withdrawal position, respectively. The use of the above optimal transition trajectory is to avoid post-withdrawal oscillations, and obtain a smooth probe displacement in the online profile design later.

Through the above test, the following probe velocity and characteristic probe positions are extracted [see Fig. 6(a) and (c)]: (1) the velocity of the probe displacement profile, $v_{w,\text{test}}(t) = \dot{z}_{w,\text{test}}(t)$, for $t \in [0,\, T_{w,\text{init}}]$; (2) the end-of-repulsive position, $Z_{w,r}$; and (3) the loss-of-contact position, $Z_{w,a}$. $Z_{w,r}$, and $Z_{w,a}$ are the initial choice of the corresponding probe position in the online iterative optimization later, respectively. The above quantification is robust, as small variations in the identification will not affect the optimization of the desired withdrawal profile. As before, the three-step FIS process is employed to optimize the withdrawal profile online. We start with the first step next.

2) Online Design the Desired Probe Withdrawal Profile: Based on the characteristic probe positions quantified above, the desired probe withdrawal profile in each of the jth FIS process, $z^j_w(\cdot)$, is designed phase-by-phase in sequence [see Fig. 6(b) and (d)]. First, for the repulsive phase, the desired probe displacement profile is chosen as the measured one in the initial test, $z_{w,\text{test}}(t)$, as

$$z^j_{w,rp}(t) = z_{w,\text{test}}(t), \quad \text{for } t \in [0,\, t^j_{rap}] \qquad (14)$$

where t^j_{rap} is the time instant for the final probe position in the repulsive phase, $Z^j_{w,r}$, i.e., $z^j_{w,rp}(t^j_{\text{rap}}) = Z^j_{w,r}$.

Then, for the attractive phase, the desired probe displacement profile is designed by using the probe velocity, $v^j_{w,s}$

$$z^j_{w,tr}(t) = v^j_{w,s}t, \quad \text{for } t \in [t^j_{\text{rap}},\, t^j_{tr,i}] \qquad (15)$$

where, to ensure a smooth repulsive-to-attractive transition, the probe velocity, $v^j_{w,s}$, is obtained as

$$v^j_{w,s} = \begin{cases} \Phi(t,\, B^j_{of},\, T_{\text{con}}), & t \in [t^j_{\text{rap}},\, t^j_{\text{con}}] \\ v^j_c, & t \in [t^j_{\text{con}},\, t^j_{tr,i}] \end{cases} \qquad (16)$$

with $\Phi(\cdot)$ the velocity transition profile obtained via the optimal transition trajectory design [see (8)], for the given velocity transition time, $T_{\text{con}} = t^j_{\text{con}} - t^j_{\text{rap}}$, and given boundary condition $B^j_{of} = (\xi(t^j_{\text{rap}}),\, \xi(t^j_{\text{con}}))$, where $\xi(t^j_{\text{rap}}) = [v_{w,\text{test}}(t^j_{\text{rap}}),\, \dot{v}_{w,\text{test}}(t^j_{\text{rap}})]^T$, $\xi(t^j_{\text{con}}) = [v^j_c,\, 0]^T$. In (16), t^j_{con} is the final time instant of the velocity transition profile, and v^j_c is the constant probe velocity obtained via the FIS process below, respectively.

Next, for the final phase, the desired probe displacement profile is obtained via the optimal transition trajectory design,

$$z^j_{w,fl}(t) = \Phi(t,\, B^j_{of},\, T_{wtr,t}), \qquad \text{for } t \in [t^j_{tr,i},\, t^j_{tr,f}] \quad (17)$$

with a given withdrawal time period, $T_{wtr,t} = t^j_{tr,f} - t^j_{tr,i}$, and boundary condition $B^j_{of} = (\xi(t^j_{tr,i}),\, \xi(t^j_{tr,f}))$, where $\xi(t^j_{tr,i}) = [Z^j_{w,a},\, v^j_c]^T$, $\xi(t^j_{tr,f}) = [Z_{w,f},\, 0]^T$, with $t^j_{tr,i}$ and $t^j_{tr,f}$ the time instant corresponding to the starting position of the final phase, $Z^j_{w,a}$, and the final withdrawal position, $Z_{w,f}$, respectively. The smooth transition from the attractive phase to the final phase is guaranteed by the boundary conditions used in the optimal transition trajectory design.

Finally, the entire desired probe withdrawal profile for the jth design update is obtained by concatenating the above three profiles together in order

$$z^j_w(t) = \left[z^j_{w,rp}(t),\, z^j_{w,tr}(t),\, z^j_{w,fl}(t)\right], \quad \text{for } t \in [0,\, t^j_{tr,f}]. \qquad (18)$$

Then, the final probe position in the repulsive phase, $Z^j_{w,r}$, the constant probe velocity in the attractive phase, v^j_c, and the starting probe position in the final phase, $Z^j_{w,a}$, are tuned through the FIS process, to optimize the probe displacement profile in the corresponding phase, $z^j_{w,rp}(t)$, $z^j_{w,tr}(t)$, and $z^j_{w,fl}(t)$, respectively.

3) Objective WO-I. Online-Minimize the Adhesive Force: The probe velocity in the attractive phase is tuned online to minimize the peak adhesive force via the FIS process. During the tuning process, the probe profiles in the preceding repulsive and the following final phase are maintained the same as those obtained in the initial design, i.e., obtained by using $Z_{w,r}$ and $Z_{w,a}$ in (14) and (17), respectively. Specifically, in the jth FIS searching/update process, the jth constant probe velocity, v^j_c, is searched via the FIS process

$$v^j_c = \Gamma_{\text{Fib}}(z^{j-1}_w(t,\, v^{j-1}_c),\, \|F^{j-1}_{Adh}(\cdot)\|_\infty) \qquad (19)$$

where $v^{j-1}_c \in [v^{j-1}_{c,l},\, v^{j-1}_{c,h}]$ is the $(j-1)$th constant probe velocity, with $v^{j-1}_{c,l}$ and $v^{j-1}_{c,h}$ the lower and upper bounds of the searching interval, respectively, and $\|F^{j-1}_{Adh}(\cdot)\|_\infty$ is the peak

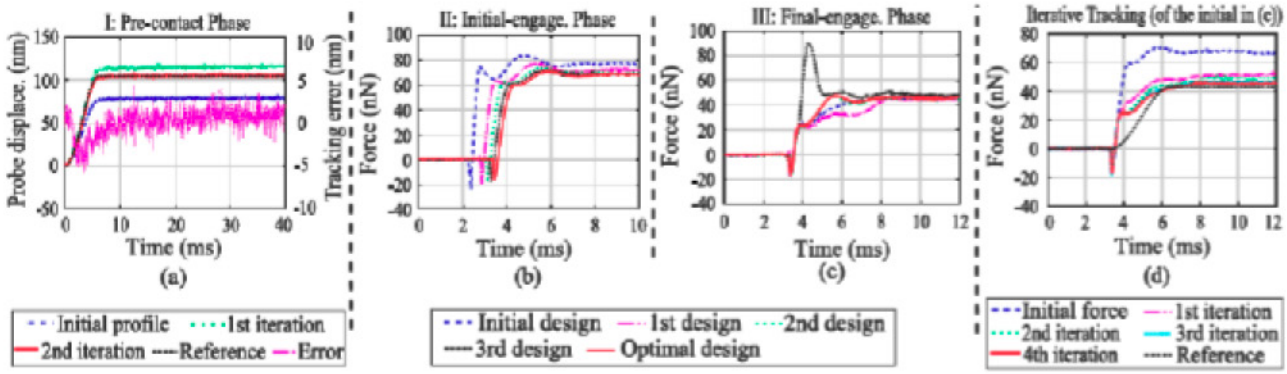

Fig. 7. (a: left axis) Iterative tracking of the desired probe displacement in the pre-contact phase along with (a: right axis) the tracking error in the last iteration. (b) Updates of the probe force profile in the initial-engagement phase via the FIS process. (c) Updates of the probe force profile in the final engagement phase via the FIS process. (d) The corresponding online tracking of the desired force profile in the initial design in (c) via MIIC, respectively, on the PDMS sample with the desired force load at 47 nN.

adhesive force, measured when the desired probe withdrawal profile, $z_w^{j-1}(t,\, v_c^{j-1})$, is tracked accurately by using the MIIC technique, respectively. The jth constant probe velocity v_c^j is used to update the probe displacement profile in the attractive phase via (15) and (16), and obtain the entire desired probe withdrawal profile through concatenation [see (18)].

4) Objective WO-II. Online-Optimize the Repulsive Transition Profile: Next, the final probe position in the repulsive phase, $Z_{w,r}^j$, is tuned via the FIS process to minimize the total withdrawal time without increasing the peak adhesive force. The optimal constant probe velocity, v_c^*, in the attractive phase and probe withdrawal profile in the final phase obtained in Objective WO-I are maintained. Specifically, in the jth FIS searching/update process, the jth repulsive final position, $Z_{w,r}^j$, is searched online to minimize the cost function $J_{z_w}^j(\cdot)$ in (4),

$$Z_{w,r}^j = \Gamma_{\text{Fib}}(z_w^{j-1}(t,\, Z_{w,r}^{j-1}),\, J_{z_w}^{j-1}(\|F_{Adh}^{j-1}(\cdot)\|_\infty,\, T_w^{j-1})) \tag{20}$$

where $Z_{w,r}^{j-1} \in [Z_{w,rl}^{j-1},\, Z_{w,rh}^{j-1}]$ is the $(j-1)$th final position of the repulsive phase, with $Z_{w,rl}^{j-1}$ and $Z_{w,rh}^{j-1}$ the lower and upper bounds of the searching interval, respectively. $\|F_{\text{Adh}}^{j-1}(\cdot)\|_\infty$ and T_w^{j-1} are the peak adhesive force and the total withdrawal time, measured when the desired probe withdrawal profile, $z_w^{j-1}(t,\, Z_{w,r}^{j-1})$, is tracked accurately by using the MIIC technique, respectively.

The weights in the cost function $J_{z_w}^{j-1}(\cdot)$ are tuned (after the initial searching interval, $[Z_{w,rl}^0,\, Z_{w,rh}^0]$, is chosen appropriately) to ensure that the force in the repulsive phase does not exceed the peak adhesive force. The jth repulsive final position, $Z_{w,r}^j$, is used to update the probe displacement profile in the repulsive phase via (14), and obtain the entire desired probe withdrawal profile through concatenation [see (18)].

5) Objective WO-III. Online-Optimize the Final Withdrawal Profile: Similarly, the total withdrawal time is further minimized by online-tuning the starting probe position in the final phase via the FIS process, under the condition that the peak adhesive force is closely maintained around the optimal peak adhesive force, F_{Adh}^*. The optimal constant probe velocity, v_c^*, and the optimal repulsive final position, $Z_{w,r}^*$, obtained in Objectives WO-I and WO-II are maintained. Specifically, the jth starting position of the final phase, $Z_{w,a}^j$, is searched online to minimize the cost function $J_{z_w}^j(\cdot)$ of (4) via the FIS searching/update process,

$$Z_{w,a}^j = \Gamma_{\text{Fib}}(z_w^{j-1}(t,\, Z_{w,a}^{j-1}),\, J_{z_w}^{j-1}(\|F_{Adh}^{j-1}(\cdot)\|_\infty,\, T_w^{j-1})) \tag{21}$$

where $Z_{w,a}^{j-1} \in [Z_{w,al}^{j-1},\, Z_{w,ah}^{j-1}]$ is the $(j-1)$th starting position of the final phase, with $Z_{w,al}^{j-1}$, $Z_{w,ah}^{j-1}$ the lower and upper bounds of the searching interval, respectively, and $z_w^{j-1}(t,\, Z_{w,a}^{j-1})$ is the desired probe withdrawal profile to track by using the MIIC technique, respectively. Then, the jth starting position of the final phase, $Z_{w,a}^j$, is used to update the probe displacement profile in the final phase via (17), and obtain the entire desired probe withdrawal profile via concatenation [see (18)].

Finally, the optimal control inputs, each corresponding to Objective WO-I, WO-II, and WO-III, respectively, are concatenated together to yield the control input for the entire withdrawal process. The smoothness of the probe withdrawal profile is guaranteed by the smoothness and precision tracking of the desired probe displacement profile.

III. Experimental Demonstration

The proposed LOS-RE and LOS-RW techniques were illustrated through AFM experiments. We start by describing the experimental setup.

A. Experimental Setup

The experiments were performed on a commercial AFM system (Dimension FastScan, Bruker Inc.), in which the piezoelectric actuators can be directly controlled via external drives, and the cantilever displacement (z-sensor signal) and the probe–sample interaction force (cantilever deflection) can be directly measured. The Matlab-xPC-target, combined with a data acquisition system, was used to implement the algorithms and process the data. The sampling rate was set at 25 kHz and 10 kHz for the probe engagement and withdrawal experiment (under the data acquisition limitation), respectively.

A PDMS sample made by mixing Sylgard 184 silicone elastomer base and curing agent together at a mass ratio of 15:1 was

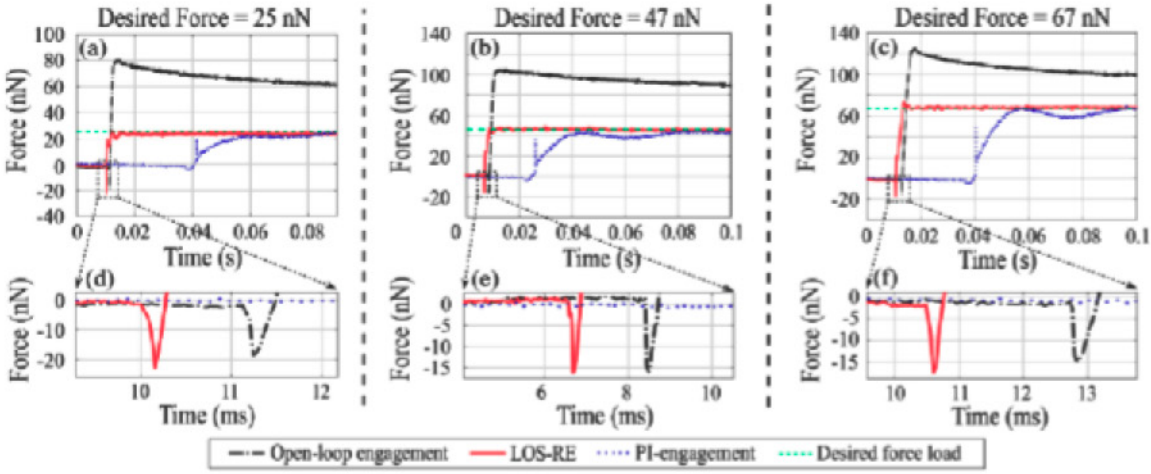

Fig. 8. Comparison of (a)–(c) the probe force, and (d)–(f) the zoomed-in view of the "snap-in" force in the dashed box above, obtained when using the proposed LOS-RE method, the open-loop engagement, and the PI-engagement, on the PDMS sample for the desired force load of 25, 47, and 67 nN, respectively.

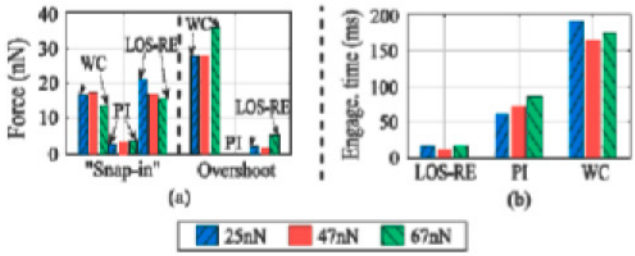

Fig. 9. Comparison of (a) the probe force, and (b) the total engagement time obtained when using the proposed LOS-RE method, the open-loop engagement (WC), and the PI-engagement (PI), on the PDMS sample for the desired force load of 25, 47, and 67 nN, respectively.

used as the test sample. The PDMS sample is hydrophobic, with an elastic modulus of around 1.3 MPa. A cantilever with a spring constant of 0.8 N/m (model: FastScan-C, Bruker Inc.) was used.

B. Learning-Based Online-Searching Rapid Probe Engagement: Implementation and Results

First, the characteristic probe positions of the engagement process were quantified through an experiment test (see Section II-C.1). Then, to achieve rapid precontact probe approach (Objective EO-I), the desired probe displacement trajectory for the precontact phase was designed by using the pre-contact time at 4 ms and tracked online by using the MIIC technique (see Section II-C.2). The convergence was reached with three iterations (with the relative RMS error less than 4%), as shown in Fig. 7(a). Next, to minimize the peak "snap-in" force (Objective EO-II), the time period of the initial-engagement phase was online-optimized through the proposed FIS process (see Section II-C.3). The desired probe displacement profile for the initial-engagement phase was updated by using the initial-engagement time and accurately tracked online by using the MIIC technique. The convergence was reached with two iterations (with the relative RMS error less than 5%). A total number of $N = 4$ updates (with $\lambda = 0.05$) was implemented

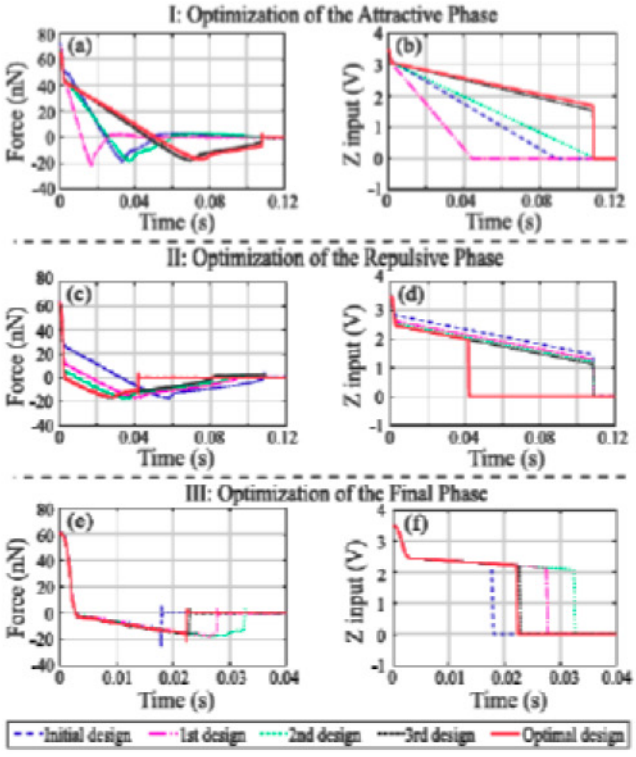

Fig. 10. (a), (c), and (e) Updates of the probe force and (b), (d), and (f) the control input in the LOS-RW process to achieve Objectives WO-I, WO-II, and WO-III on the PDMS sample with initial force load at ~60 nN, respectively.

in the FIS process, and the corresponding probe force profiles were measured and shown in Fig. 7(b). Finally, after Objectives EO-I and EO-II had been achieved, the time period of the final-engagement phase was also online-optimized to minimize the peak overshoot force and reach the desired force load at 47 nN (Objective EO-III) via the proposed FIS process (see Section II-C.4). The desired probe force profile was updated by using the final-engagement time and tracked accurately online

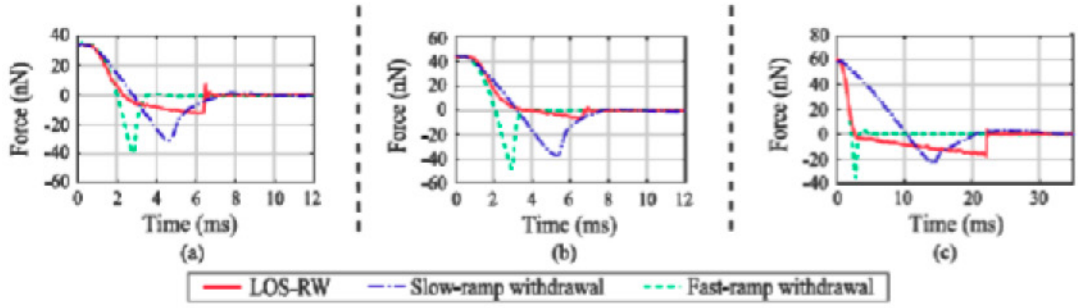

Fig. 11. Comparison of (a)–(c) the probe force obtained by using the proposed LOS-RW method, the slow-ramp withdrawal, and the fast-ramp withdrawal, respectively, on the PDMS sample for the initial force load of ~34, ~44, and ~60 nN, respectively.

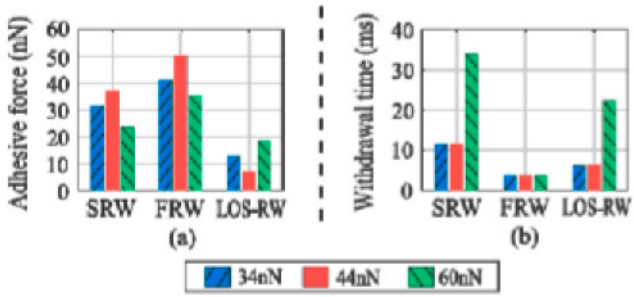

Fig. 12. Comparison of (a) the adhesive force and (b) the total withdrawal time obtained by using the proposed LOS-RW method, the slow-ramp withdrawal (SRW) and the fast-ramp withdrawal (FRW), respectively, on the PDMS sample for the initial force load of ~34, ~44, and ~60 nN, respectively.

by using the MIIC technique. The convergence was reached after five iterations (with the relative RMS error between the desired and measured force load less than 5%). A total of four FIS online updates were conducted, and the probe force profiles were measured and shown in Fig. 7(c). As an example, the iterative tracking of the desired force profile in the initial design is presented in Fig. 7(d). Then, all the obtained optimal control input profiles for the three phases were concatenated together to obtain that for the probe engagement process.

For comparison, the probe engagement without control (i.e., the open-loop engagement) and with the PI control (called the *PI-engagement* below), respectively, were also measured in the experiment under the same experimental conditions (e.g., the same sample location, the same desired force load). For the open-loop engagement, a smooth probe displacement profile was online designed and tracked to transit the probe from the tip–sample interaction border at ~538 nm to reach the estimated probe position corresponding to the desired force load [see (22)] within ~6 ms. For the PI-engagement, a ramp input with a velocity of ~30 nm/ms was applied initially, and then the PI control was switched on once the contact force was detected until the desired force load was reached. The experimental results via these three methods were also obtained for two other desired force loads of 25 and 67 nN, respectively. The probe force for these three methods with three desired force loads was measured and shown in Fig. 8(a)–(c), where a zoomed-in view of the "snap-in" forces is shown in Fig. 8(d)–(f). The peak "snap-in" force, peak overshoot force, and the total engagement time were also quantified and compared in Fig. 9(a) and (b), respectively.

C. Learning-Based Online-Searching Rapid Probe Withdrawal: Implementation and Results

Next, the proposed LOS-RW technique was implemented. The initial stable contact was established a priori at a force load of ~60 nN. The characteristic probe positions were estimated experimentally through a withdrawal test (see Section II-D.1). First, the probe velocity in the attractive phase was optimized to minimize the peak adhesive force online (Objective WO-I) via the FIS process (see Section II-D.3). The desired withdrawal profile was updated by using the probe velocity and tracked accurately online by using the MIIC technique. The convergence was reached with two iterations (with the relative RMS error less than 5%). The FIS process was stopped after four design updates, and the corresponding probe force profiles and control inputs were measured and shown in Fig. 10(a) and (b), respectively. Then, the repulsive final position was also online-optimized by minimizing the cost function in (4) (Objective WO-II) via the FIS process (see Section II-D.4). The desired withdrawal profile was updated by using the repulsive final position and tracked accurately online by using the MIIC technique. The convergence was reached in two iterations (with the relative RMS error less than 5%). The FIS process was terminated after four design updates, and the probe force profiles and control inputs were measured and shown in Fig. 10(c) and (d), respectively. Finally, to further minimize the total withdrawal time, the starting position of the final phase was optimized (Objective WO-III) via the FIS process (see Section II-D.5). The desired withdrawal profile was updated by using the starting position and tracked accurately online by using the MIIC technique. The convergence was reached in two iterations (with the relative RMS error less than 5%). Four FIS online updates were conducted, and the probe forces and control inputs are shown in Fig. 10(e) and (f), respectively. The optimal control input profiles obtained in the above three phases were concatenated together to obtain the entire optimal input profile for the probe withdrawal.

For comparison, the ramp withdrawal experiments at two different velocities under the same initial and final probe positions, respectively, were also conducted. One fast ramp velocity was set at ~20 nm/ms (called the *fast-ramp withdrawal* below). The

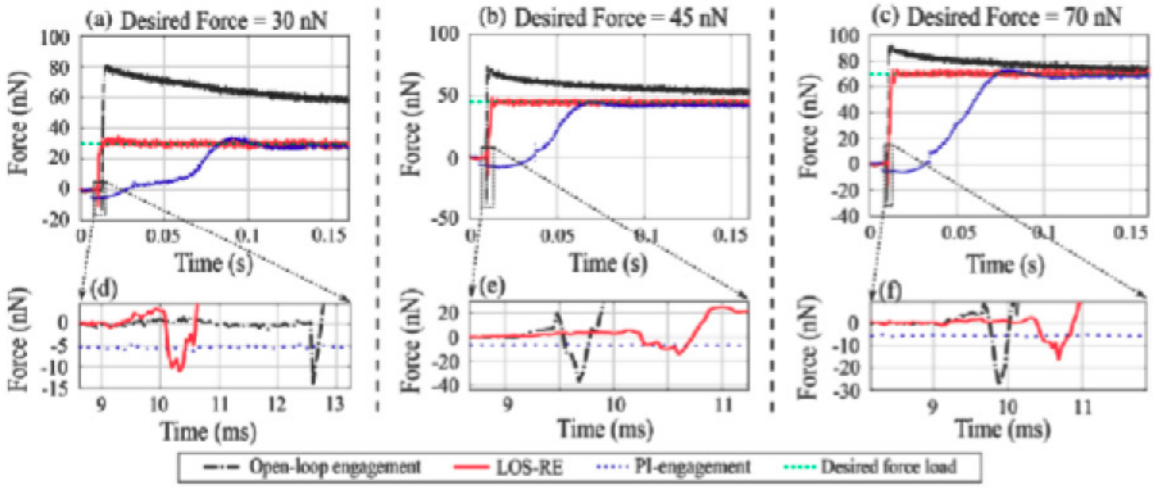

Fig. 13. Comparison of (a)–(c) the probe force, and (d)–(f) the zoomed-in view of the "snap-in" force in the dashed box above, obtained by using the proposed LOS-RE method, the open-loop engagement and the PI-engagement, on the dental silicone sample for the desired force load of 30, 45, and 70 nN, respectively.

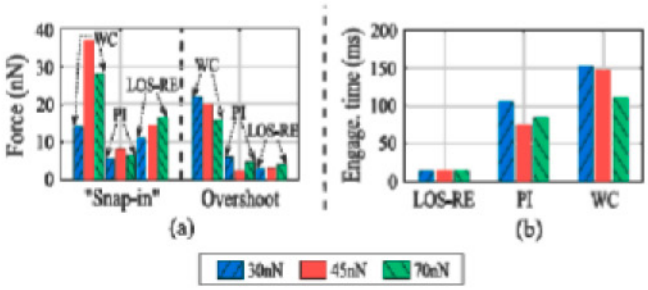

Fig. 14. Comparison of (a) the probe force and (b) the total engagement time obtained by using the proposed LOS-RE method, the open-loop engagement (WC), and the PI-engagement (PI), on the dental silicone sample for the desired force load of 30, 45, and 70 nN, respectively.

other velocity was chosen such that the time instant corresponding to the loss-of-contact position matched well with that of the proposed LOS-RW process (called the *slow-ramp withdrawal* below). Moreover, the experiments via these three methods were also implemented at two other initial stable contacts at ~34 nN and ~44 nN, respectively. The probe forces for these three methods are compared in Fig. 11(a)–(c) for the three initial force loads, respectively. The peak adhesive force and the total withdrawal time were quantified and compared in Fig. 12(a) and (b), respectively.

IV. Results and Discussion

The experimental results demonstrated that, by using the proposed LOS-RE approach, the proposed Objectives EO-I, EO-II, and EO-III were achieved. First, the total engagement time was substantially reduced by over 85.0% and 93.4%, when compared to that of the PI-engagement and the open-loop engagement, respectively, from 72.0 ms (PI-engagement) and 165.0 ms (open-loop) to 10.8 ms, respectively [see Figs. 8(b) and 9(b)]. Also, by using the LOS-RE process, the desired force load of ~47 nN was reached with an error less than 5%, whereas the open-loop engagement could not achieve the desired force load. Furthermore, the peak overshoot force was also reduced dramatically to 1.7 nN, an over 93.9% reduction from that in the open-loop engagement at 28.0 nN [see Figs. 8(b) and 9(a)]. Although the peak "snap-in" force and the overshoot force were smaller when using the PI-engagement [see Figs. 8(b) and (c) and 9(a)], such a force reduction was accompanied with a much larger engagement time—over 5.7 times. Such a long time engagement is not suitable in applications where rapid probe engagement is needed, such as the piecewise-scanning-based imaging [1] or the discrete nanomechanical mapping [2]. Contrarily, by using the proposed method, the engagement time was reduced by over 85%. The proposed method also provides an optimal trade-off between the interaction force and the engagement time, i.e., the interaction force can be further reduced by allowing a larger engagement time. These results—the dramatic reduction of the force (over the open-loop engagement) and the engagement time (over both the open-loop and PI-control ones)—were also observed in the other two force load cases, as can be seen clearly in Figs. 8 and 9. Therefore, the proposed LOS-RE process was highly efficient and effective in achieving rapid probe engagement with the interaction force online-minimized.

The experimental results also demonstrated that by using the proposed LOS-RW approach, the proposed Objectives WO-I, WO-II, and WO-III were achieved. First, by using the LOS-RW process, the peak adhesive force of the probe withdrawal was reduced by over 21.7% and 47.7% compared to that when using the slow- and fast-ramp withdrawal, respectively, from 23.5 nN (slow-ramp) and 35.2 nN (fast-ramp) to 18.4 nN, respectively [see Figs. 11(c) and 12(a)]. Furthermore, the total withdrawal time was reduced dramatically to 22.3 ms, an over 34.4% reduction from that of the slow-ramp withdrawal at 34 ms. Although the total withdrawal time was smaller when using the fast-ramp withdrawal [see Figs. 11(c) and 12(b)], such a time reduction was obtained at the cost of a much larger peak adhesive force—the

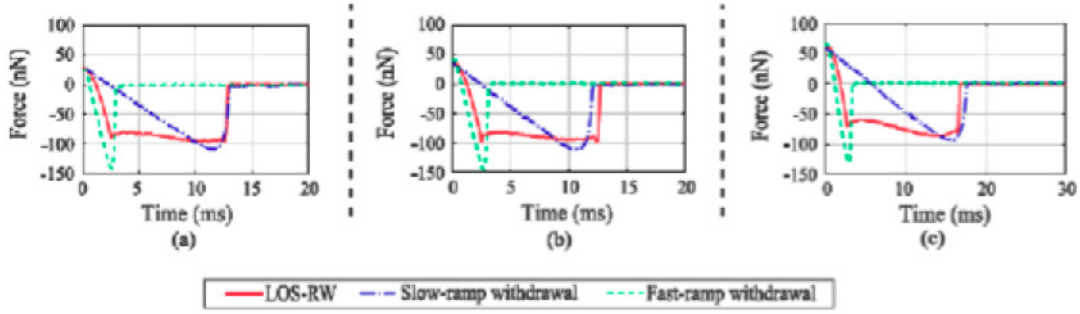

Fig. 15. Comparison of (a)–(c) the probe force obtained by using the proposed LOS-RW method, the slow-ramp withdrawal, and the fast-ramp withdrawal, on the dental silicone sample for the initial force load of ~25, ~40, and ~60 nN, respectively.

peak adhesive force increased by over 91.3%. Large adhesive force deforms and damages soft samples, especially live biological specimens, and becomes even worse in applications where repetitive withdrawal operations are required [1], [2]. Contrarily, by using the proposed method, the adhesive force was reduced by over 48%. Moreover, the proposed method provides an optimal trade-off between the adhesive force and the withdrawal time, i.e., the adhesive force can be further reduced by allowing a longer withdrawal time. These results—the dramatic reduction of the adhesive force (over both the fast-and slow-ramp withdrawal) and the total withdrawal time (over the slow-ramp withdrawal)—were also observed in other two initial force load cases, as can be seen clearly in Figs. 11 and 12. Therefore, the proposed LOS-RW process was highly efficient and effective in achieving rapid probe withdrawal with the adhesive force online-minimized.

To further validate the efficacy of the proposed approach, experiments were also conducted on a hydrophilic dental silicone sample prepared by using nanoimprint lithography with a quasicrystalline stamp. The above three engagement methods were applied under three different force loads at 30 nN, 45 nN, and 70 nN, respectively. In the proposed LOS-RE process, the convergence of tracking the desired displacement and force profile were reached with two and five iterations, respectively (with the relative RMS error less than 5%). The corresponding probe forces measured are compared in Fig. 13(a)–(c), with a zoomed-in view of the "snap-in" forces shown in Fig. 13(d)–(f), respectively. The quantified peak "snap-in" force, overshoot force, and total engagement time are also presented in Fig. 14(a) and (b). The probe withdrawal experiment was also conducted on this sample by using the above three withdrawal methods at three different initial force loads of ~25, ~40, and ~60 nN, respectively. In the proposed LOS-RW process, the convergence of tracking the desired displacement profile was reached with two iterations (with the relative RMS error less than 5%). The measured probe forces are shown in Fig. 15(a)–(c), and the quantified peak adhesive force and the total withdrawal time are summarized in Fig. 16(a) and (b).

The experimental results obtained on the dental silicone sample also showed similar improvements as those obtained on the PDMS sample previously. Both the probe–sample interaction force and the engagement or withdrawal time were reduced by using the proposed approach, as can be seen in Figs. 13–16,

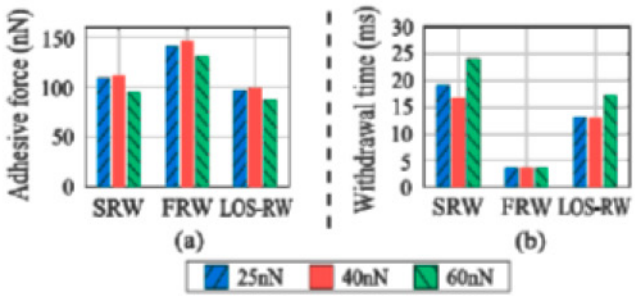

Fig. 16. Comparison of (a) the adhesive force and (b) total withdrawal time obtained by using the proposed LOS-RW method, the slow-ramp withdrawal (SRW), and the fast-ramp withdrawal (FRW), on the dental silicone sample for the initial force load of ~25, ~40, and ~60 nN, respectively.

respectively. Thus, this experiment further demonstrated the proposed method in achieving rapid probe engagement and withdrawal. A preliminary work of using the proposed approach in AFM applications has been illustrated recently for discrete nanomechanical mapping [2].

V. Conclusion

An online-searching-based learning approach to achieve rapid probe engagement and withdrawal with the probe–sample-interaction force minimized is proposed. The proposed approach explored the idea of piecewise sequential optimization to tackle the challenges in the highly nonlinear stiff force–distance relationship involved. The probe engagement and withdrawal process had been partitioned into three phases and online-optimized in sequence. A Fibonacci-based iterative optimization approach had been proposed for online optimization. The proposed approach was illustrated through experimental implementations on a polydimethylsiloxane (PDMS) sample and a dental silicone sample.

Appendix A
Modeling-Free Iterative Learning Control Technique

The MIIC technique [15] is used to achieve precision tracking of a given desired trajectory $y_d(t)$. Specifically, the MIIC

algorithm is given in the frequency domain as

$$u_{1,tr}(j\omega) = \alpha y_d(j\omega), \tag{22}$$

$$u_{k+1,tr}(j\omega) = \begin{cases} \frac{u_{k,tr}(j\omega)}{y_{k,tr}(j\omega)} y_d(j\omega), & \text{if } k \geq 1, y_{k,tr}(j\omega) \neq 0 \\ 0, & \text{otherwise} \end{cases} \tag{23}$$

where, respectively, α is the reciprocal of the dc-gain of the z-axis piezoelectric actuator, $y_{k,tr}(j\omega)$ and $u_{k,tr}(j\omega)$ are the Fourier transform of the measured trajectory (i.e., the probe displacement or the probe force) and the control input applied to the z-axis piezo actuator in the kth iteration, and $y_d(j\omega)$ is the Fourier transform of the desired trajectory to track. The MIIC algorithm is iteratively implemented until the convergence is reached, i.e., the tracking error, $\|y_{k,tr}(\cdot) - y_d(\cdot)\|_2$, cannot be further reduced. In practice, usually only a few iterations (<5) are needed [20].

Appendix B
Online Fibonacci-Based Optimization

In the proposed FIS process, the Fibonacci algorithm is utilized to update the parameter to be optimized,

$$V^j = \Gamma_{\text{Fib}}(\Psi^{j-1}(t, V^{j-1}), \mathscr{F}^{j-1}(V^{j-1})) \tag{24}$$

where V^j is the parameter to be optimized in the jth update, $\mathscr{F}(V)$ is the response value that is minimized through the optimization of V, and $\Psi(t, V)$ is the trajectory (i.e., function) that depends on the parameter V, respectively. Moreover, $\mathscr{F}(V)$ is measured when the trajectory $\Psi(t, V)$ is tracked, i.e.

$$\text{Tracking}(\Psi(t, V)) \xrightarrow{\text{MIIC}} \mathscr{F}(V). \tag{25}$$

First, for each jth design update ($2 \leq j \leq N$, N: the prechosen total number of search times), let V_l^{j-1} and V_h^{j-1} be the lower and upper bounds of the search interval of V^{j-1}, respectively, V_{opt}^{j-1} be the intermediate "optimal" parameter, and $\mathscr{F}_{\text{opt}}^{j-1}(V_{\text{opt}}^{j-1})$ be the corresponding intermediate "optimal" response value, respectively. Then, after the $(j-1)$th desired trajectory, $\Psi^{j-1}(t, V^{j-1})$, has been tracked accurately, the response value, $\mathscr{F}^{j-1}(V^{j-1})$, is measured and compared to the intermediate "optimal" response value. When $\mathscr{F}^{j-1}(V^{j-1}) > \mathscr{F}_{\text{opt}}^{j-1}(V_{\text{opt}}^{j-1})$, we set

$$\begin{aligned} V_l^j = V_l^{j-1}, \quad V_h^j = V^{j-1}, \quad V^j = V_l^j + \rho_j \Delta_j \\ \text{if } V^{j-1} > V_{\text{opt}}^{j-1} \text{ or} \\ V_l^j = V^{j-1}, \quad V_h^j = V_h^{j-1}, \quad V^j = V_h^j - \rho_j \Delta_j \\ \text{if } V^{j-1} < V_{\text{opt}}^{j-1} \end{aligned} \tag{26}$$

and keep the jth intermediate "optimal" values the same, i.e.

$$V_{\text{opt}}^j = V_{\text{opt}}^{j-1}, \quad \mathscr{F}_{\text{opt}}^j(V_{\text{opt}}^j) = \mathscr{F}_{\text{opt}}^{j-1}(V_{\text{opt}}^{j-1}) \tag{27}$$

where, respectively, Δ_j is the jth search interval length, $\Delta_j = V_h^j - V_l^j$, and ρ_j is the update coefficient determined by $\rho_j = 1 - F_{N-j+1}/F_{N-j+2}$, $j = 1, 2, \ldots, N-1$, with the Fibonacci sequence $F_1, F_2, \cdots$ given by

$$F_0 = F_1 = 1, \; F_j = F_{j-1} + F_{j-2}, \quad j = 2, 3, \ldots, N+1. \tag{28}$$

The length of the Fibonacci sequence N is determined by the prechosen threshold level δ for the optimal parameter via $(1 + 2\lambda)/F_{N+1} \leq \delta/\Delta_{\text{init}}$, with λ a prechosen threshold to update $\rho_N = 0.5 - \lambda$ in the Nth step.

Otherwise, when $\mathscr{F}^{j-1}(V^{j-1}) < \mathscr{F}_{\text{opt}}^{j-1}(V_{\text{opt}}^{j-1})$, we set

$$\begin{aligned} V_l^j = V_{\text{opt}}^{j-1}, \quad V_h^j = V_h^{j-1}, \quad V^j = V_h^j - \rho_j \Delta_j \\ \text{if } V^{j-1} > V_{\text{opt}}^{j-1} \text{or} \\ V_l^j = V_l^{j-1}, \quad V_h^j = V_{\text{opt}}^{j-1}, \quad V^j = V_l^j + \rho_j \Delta_j \\ \text{if } V^{j-1} < V_{\text{opt}}^{j-1} \end{aligned} \tag{29}$$

$$V_{\text{opt}}^j = V^{j-1}, \quad \mathscr{F}_{\text{opt}}^j(V_{\text{opt}}^j) = \mathscr{F}^{j-1}(V^{j-1}). \tag{30}$$

At the beginning, the lower and upper bounds of the search interval, V_l^{init} and V_h^{init}, will be chosen a priori, and the parameter to be optimized for the initial and the first design update, V^0, V^1, are determined as

$$V^0 = V_l^{\text{init}} + \rho_1 \Delta_{\text{init}}, \quad V^1 = V_h^{\text{init}} - \rho_1 \Delta_{\text{init}}. \tag{31}$$

After the initial and the first design of the desired trajectory, $\Psi^0(t, V^0)$ and $\Psi^1(t, V^1)$, have been tracked accurately, the response values, $\mathscr{F}^0(V^0)$, and $\mathscr{F}^1(V^1)$, are measured and used to determine the first intermediate "optimal" parameter and the intermediate "optimal" response value

$$\begin{aligned} V_{\text{opt}}^1 = V^0, \quad \mathscr{F}_{\text{opt}}^1(V_{\text{opt}}^1) = \mathscr{F}^0(V^0) \\ \text{if } \mathscr{F}^1(V^1) > \mathscr{F}^0(V^0) \text{ or} \\ V_{\text{opt}}^1 = V^1, \quad \mathscr{F}_{\text{opt}}^1(V_{\text{opt}}^1) = \mathscr{F}^1(V^1) \\ \text{if } \mathscr{F}^1(V^1) < \mathscr{F}^0(V^0). \end{aligned} \tag{32}$$

These values serve as the initial conditions needed to start the Fibonacci search process described above.

Acknowledgment

The authors would like to thank Prof. Jonathan Singer and Arielle Marie Gamboa for the sample preparation.

References

[1] R. A. Braker, Y. Luo, L. Y. Pao, and S. B. Andersson, "Hardware demonstration of atomic force microscopy imaging via compressive sensing and μ-path scans," in *Proc. Annu. Amer. Control Conf.*, 2018, pp. 6037–6042.

[2] J. W. Qingze Zou and C. Su, "Rapid broadband discrete nanomechanical mapping on atomic force microscope," in *Proc. Annu. Amer. Control Conf., IEEE*, 2019, pp. 2227–2232.

[3] Z. Wang, J. Tan, Q. Zou, and W. Jiang, "Mechanical-plowing-based high-speed patterning on hard material via advanced-control and ultrasonic probe vibration," *Rev. Sci. Instrum.*, vol. 84, no. 11, 2013, Art. no. 113704.

[4] H.-J. Butt, B. Cappella, and M. Kappl, "Force measurements with the atomic force microscope: Technique, interpretation and applications," *Surf. Sci. Rep.*, vol. 59, no. 1, pp. 1–152, 2005.

[5] P. Eaton and P. West, *Atomic Force Microscopy*. New York, NY, USA: Oxford University Press, 2010.

[6] H. Xie, H. Zhang, J. Song, X. Meng, Y. Wen, and L. Sun, "High-precision automated micromanipulation and adhesive microbonding with cantilevered micropipette probes in the dynamic probing mode," *IEEE/ASME Trans. Mechatronics*, vol. 23, no. 3, pp. 1425–1435, Jun. 2018.
[7] V. J. Morris, A. R. Kirby, and A. P. Gunning, *Atomic Force Microscopy for Biologists*. Singapore: World Scientific, 2010.
[8] G. Han, B. Lin, and Y. Lin, "Reconstruction of atomic force microscopy image using compressed sensing," *Micron*, vol. 105, pp. 1–10, 2018.
[9] X. Zhang, J. Ren, J. Wang, S. Li, Q. Zou, and N. Gao, "Receptor-mediated endocytosis generates nanomechanical force reflective of ligand identity and cellular property," *J. Cellular Physiol.*, vol. 233, no. 8, pp. 5908–5919, 2018.
[10] R. Carter *et al.*, "Stomatal opening involves polar, not radial, stiffening of guard cells," *Current Biol.*, vol. 27, no. 19, pp. 2974–2983, 2017.
[11] R. Garcia and A. San Paulo, "Attractive and repulsive tip-sample interaction regimes in tapping-mode atomic force microscopy," *Phys. Rev. B*, vol. 60, no. 7, 1999, Art. no. 4961.
[12] Q. Xu, M. Li, J. Niu, and Z. Xia, "Dynamic enhancement in adhesion forces of microparticles on substrates," *Langmuir*, vol. 29, no. 45, pp. 13743–13749, 2013.
[13] K. Karrai and I. Tiemann, "Interfacial shear force microscopy," *Phys. Rev. B*, vol. 62, no. 19, 2000, Art. no. 13174.
[14] H. Wang, Q. Zou, and H. Xu, "Inversion-based optimal output tracking–transition switching with preview for nonminimum-phase linear systems," *Automatica*, vol. 48, no. 7, pp. 1364–1371, 2012.
[15] K.-S. Kim and Q. Zou, "A modeling-free inversion-based iterative feedforward control for precision output tracking of linear time-invariant systems," *IEEE/ASME Trans. Mechatronics*, vol. 18, no. 6, pp. 1767–1777, Dec. 2013.
[16] E. K. Chong and S. H. Zak, *An Introduction to Optimization*. Hoboken, NJ, USA: Wiley, 2013, vol. 76.
[17] Z. Wang, Q. Zou, L. Faidley, and G.-Y. Kim, "Dynamics compensation and rapid resonance identification in ultrasonic-vibration-assisted microforming system using magnetostrictive actuator," *IEEE/ASME Trans. Mechatronics*, vol. 16, no. 3, pp. 489–497, Jun. 2011.
[18] J. Wang and Q. Zou, "Rapid probe engagement and withdrawal with online minimized probe-sample interaction force in atomic force microscopy," in *Proc. ASME Dyn. Syst. Control Conf.*, Atlanta, Georgia, USA, 2018, Paper DSCC2018-9156, V001T11A004.
[19] H. Perez, Q. Zou, and S. Devasia, "Design and control of optimal scan trajectories: Scanning tunneling microscope example," *J. Dyn. Syst. Meas. Control*, vol. 126, no. 1, pp. 187–197, 2004.
[20] J. Ren and Q. Zou, "A control-based approach to accurate nanoindentation quantification in broadband nanomechanical measurement using scanning probe microscope," *IEEE Trans. Nanotechnol.*, vol. 13, no. 1, pp. 46–54, Jan. 2014.

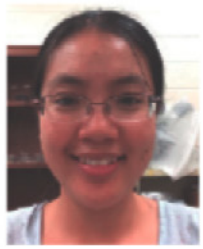

Jingren Wang received the B.S. degree in vehicle application engineering from Jilin University, China, in 2010, and the M.S. degree in vehicle engineering from the Tongji University, China, in 2013. She is currently working toward the Ph.D. degree in mechanical engineering at the Department of Mechanical and Aerospace Engineering, Rutgers University, Piscataway, NJ, USA.

Her current research interests include the online-searching learning-based nanomanipulation and the rapid discrete broadband nanomechanical mapping of soft materials.

Qingze Zou received the Ph.D. in mechanical engineering from the University of Washington, Seattle, WA, USA, in Fall 2003.

He is currently a Professor of mechanical and aerospace engineering with the Rutgers University, Piscataway, NJ, USA. Previously he was with the Iowa State University, USA. His research interests include learning-based precision tracking and motion control, control of high-speed scanning probe microscopy, nanoscale acoustic noise cancellation, recycling automation, and stomata dynamics modeling.

Dr. Zou received the NSF CAREER Award in 2009, and the O. Hugo Schuck Best Paper Award from the American Automatic Control Council in 2010. He has been an Associate Editor of *ASME Journal of Dynamic Systems, Measurement and Control*, a Senior Editor of *IEEE/ASME Transactions on Mechatronics*, and an Associate Editor of *Control Engineering Practice, and Mechatronics*. He is also a Fellow of ASME.